Transition of a small-bipolaron gas to a Fröhlich polaron in a deformable lattice

Gayan Prasad Hettiarachchi,[1,2,*] Mohd Nazlan Mohd Muhid,[3] and Halimaton Hamdan[3]
[1]*Graduate School of Engineering Science, Osaka University, Toyonaka, Osaka 560-8531, Japan*
[2]*Department of Physics, Osaka University, Toyonaka, Osaka 560-0043, Japan*
[3]*Department of Chemistry, Faculty of Science, University of Technology Malaysia, 81310 Skudai, Johor, Malaysia*

(Received 21 June 2017; revised manuscript received 27 March 2018; published 19 April 2018)

The electronic properties of guest Cs atoms in a deformable lattice are investigated at various densities n. Low values of n show optical absorptions of small bipolarons. At intermediate n values, new bands appear in the midinfrared (MIR) and high-frequency regions, which coexist with the small bipolaron bands. With a further increase in n, the small bipolaron bands become less discernible and subsequently disappear, resulting in the appearance of a Drude component superimposed on a MIR sideband suggesting a phase transition to a polaronic metal. In this itinerant phase, an approximately twofold mass enhancement is observed. This continuous transition of a gas of small bipolarons to a polaronic metal characterized by a Fröhlich polaron reveals an important part of the complex phase diagram of the metal-insulator transition in a deformable lattice.

DOI: 10.1103/PhysRevB.97.155142

I. INTRODUCTION

Polarons [1] play a key role in several phenomena at the heart of condensed-matter physics, such as high-transition-temperature (T_c) superconductivity, metal-insulator transitions (MITs), and intriguing magnetic phases with implicated polaron-correlation effects [2–9]. In clean systems, polaron formation occurs at very strong electron-lattice coupling, uncharacteristic of typical metals. Polaronic effects are more pronounced in disordered systems because slow diffusion and localization induce local-lattice deformation and symmetry breaking [10,11]. Moreover, the lattice degrees of freedom associated with a deformable lattice drastically alter the nature of the effective disorder due to local lattice deformations induced by electron-lattice coupling effects.

Many theoretical studies highlight the importance of the electron-lattice coupling strength (λ) and Frank-Condon displacements on the mobility edge [12–14] because a Hartree-type electron-lattice interaction can strongly renormalize the disorder (W), drastically affecting the random electronic potential [15,16]. The transition between small (bi)polarons (self-trapped) and delocalized states in disordered media has been a subject of debate since the discovery of localization [15,17,18]. A discontinuous transition (discontinuity being proportional to $\lambda^{2/3}$) is proposed within the adiabatic approximation [13,19] by combining the scaling theory of Emin and Holstein for polaron formation [20] with that of the Anderson localization (interacting scenario) [21]. On the other hand, the microscopic treatment of Anderson localization (noninteracting scenario) and lattice deformations due to polaronic effects in a deformable lattice proposed a continuous transition below a critical coupling strength (λ_c) with decreasing W [16]. Below λ_c, the phase diagram comprises two regions for the proposed continuous transition. At intermediate coupling, the conducting phase is characterized by extended states, which show a negative temperature coefficient of resistivity (TCR) [16]. Conventional metallic behavior is suppressed even at weak W ($W \rightarrow 0$). In the weak-coupling regime, the extended states are followed by conventional metallic behavior as $W \rightarrow 0$ [16]. Above λ_c, a mobility gap is open even at weak W.

Experimental investigations by electron-density modulation in a deformable lattice, using the host $M_{7.8-\delta}Al_{7.8}Si_{8.2}O_{32.0}$ (zeolite P [22]; M=K, Rb) as a model system, reported both discontinuous [8] and continuous transitions [23] to extended states depending on λ (controlled by changing the alkali-metal element) and W (controlled by electron-density modulation). These studies highlight that the scaling of the transition remains debatable and that theories supporting both discontinuous [13] and continuous transitions [16] apply, perhaps in different coupling regimes. As theoretically predicted, the extended states exhibited negative TCR with finite conductivity at zero temperature [23]. Further, the transition to extended states was characterized by the appearance of band(s) in the midinfrared (MIR) region, which coexist with the small bipolaron absorption bands [8,23]. In a delocalized phase characterized by extended states, electron-lattice coupling produces absorption(s) in the MIR region due to incoherent transport, which coexists with small (bi)polaron bands [23–26]. In an itinerant phase characterized by a polaronic metal, a Drude response (coherent term) appears; however, renormalized by band(s) in the MIR region (incoherent term) [25,26]. In a conventional metallic phase, a Drude response explains the charge dynamics due to coherent transport [24]. Although the aforementioned experimental studies [8,23] provide vital information toward the reconciliation of diverging theories [13,16], the observation of a conventional or polaronic metal in this model system has remained elusive, hindering the progress towards a generic theory.

In addressing this, we investigate the optical and magnetic properties of electrons in the aforementioned model system in

*hettiarachchi@hpr.stec.es.osaka-u.ac.jp

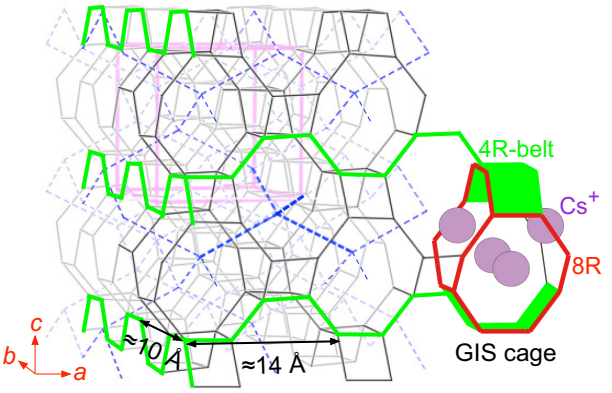

FIG. 1. The quasi-two-dimensional framework of Cs-form zeolite P. See the text for details.

a comparatively weaker coupling regime than previously investigated [8,23]. We report the continuous transition of small bipolarons to a polaronic metal by carrier-density modulation. We observe a nonmagnetic and insulating phase along with characteristic optical absorptions featuring small bipolarons. Increasing number-density of small bipolarons (decreasing W and increasing correlations) results in polaronic melting [7,27] and subsequent disappearance of the small bipolaron bands in contrast to previous studies [8,23]. This results in the appearance of a Drude component superimposed on a MIR sideband suggesting a transition to a polaronic metal. In this phase, an approximately twofold mass enhancement is observed yielding a coupling constant consistent with a Fröhlich polaron [25,28]. Based on our systematic experimental investigations [8,23], we propose a phase diagram for the MIT in a deformable lattice in the face of electron-lattice coupling and a random electronic potential.

II. EXPERIMENTAL

Quasi-two-dimensional (quasi-2D) aluminosilicate framework of zeolite P [22] formed by gismondine (GIS) cages is shown in Fig. 1. The unit cell comprises four GIS cages. The GIS cage is constructed of four eight-membered rings (8Rs) two of which are marked by the thick red lines and six four-membered rings (4Rs) marked by the shaded areas in green. The 8Rs are shared between cages forming zigzag channels along the a and b axes. The cage voids across adjacent channels form a diamond lattice as denoted by the broken lines. The 4Rs at the top and bottom of a cage (shaded areas in green) form belts along the a and b axes (green lines) resulting in a quasi-2D space. Cs cations (purple solid circles) are located at the centers of 8Rs to balance the negative charge of the framework. These provide a deformable ionic-lattice ideal for investigating electron-lattice coupling effects [9]. The Coulomb interactions between ionized valence electrons of guest Cs atoms and Cs cations (the deformable lattice) introduce electron-lattice coupling effects. This results in cationic displacements and, in turn, local lattice-deformations and drastic fluctuations in the electronic potential.

Cs-form zeolite P was obtained by ion exchange of Rb-form zeolite P [23] in a CsCl aqueous solution. The chemical formula per GIS cage obtained by inductively coupled plasma optical emission spectroscopy is $Cs_{1.65}Al_{1.95}Si_{2.05}O_{8.00}$ (Cs_2-P). This shows a deficiency of Cs cations (< nominal value of 1.95) possibly due to protonation during the ion exchange. The samples were synthesized by adsorbing accurately weighed Cs metal into Cs_2-P powder at 70 °C inside sealed glass tubes. The average number of guest Cs atoms (in effect, guest electrons) per GIS cage is denoted by n, and the chemical formula is rewritten as $Cs_{1.65+n}Al_{1.95}Si_{2.05}O_{8.00}$ (Cs_n/Cs_2-P). Samples with $n = 0.08, 0.19, 0.32, 0.41, 0.53, 0.61, 0.71, 0.79,$ and 0.87 were synthesized. The diffuse reflectance $r(\omega)$ of several series of samples was measured at room temperature using an ultraviolet-visible-near-infrared spectrometer and a Fourier transform infrared spectrometer. The optical absorption was obtained using the Kubelka-Munk transformation $k/s = (1-r)^2/2r$ [29], where k and s are the absorption and scattering coefficients, respectively. The reflectance R was obtained using the transformation $R \approx 4r/(1+r)^2$ in appropriate spectral regions demonstrating a low transmission [30]. The dc magnetization was measured using a superconducting quantum interference device magnetometer in the temperature range 1.8–300 K. The samples were sealed inside glass tubes during all measurements. There are several origins of disorder that contribute to a random electronic potential: (1) deficiency of Cs cations as observed in the chemical formula, (2) presence of Si-O-Si bonds when the Si-to-Al ratio > 1 (the Si-to-Al ratio is 1.05 in this case), (3) introduction of additional Cs cations from ionized guest Cs-atoms, and (4) local lattice deformations, i.e., cationic displacements due to electron-lattice coupling effects, being the major contributor.

III. RESULTS

The room-temperature optical absorption spectra pertaining to Cs_n/Cs_2-P at $n = 0.08$, 0.19, 0.32, 0.41, 0.53, and 0.61 are shown in Fig. 2(a). At $n = 0.08$, absorption bands appear at approximately 6600 (solid circle) and 10 500 cm^{-1} (open circle) that can be assigned to small bipolaron absorptions. One of the fingerprints of electron-lattice coupling is the formation of small (bi)polarons, which produce characteristic optical absorptions at a resonant excitation energy [24,31]. The small-polaron absorption spectrum $\alpha_{sp}(\omega)$ suggested by Emin [24] is in the form

$$\alpha_{sp}(\omega) = \frac{2(\pi)^{3/2}e^2}{m^*\omega c}\frac{t'}{\Delta}\exp\left[-\frac{(2E_b-\hbar\omega)^2}{\Delta^2}\right], \qquad (1)$$

where m^* is the electronic effective mass, c is the velocity of light, t' ($\equiv \hbar^2/2m^*a^2$) is the intersite electronic transfer energy, a is a lattice constant, Δ ($\equiv \sqrt{8E_bE_{vib}}$), and E_{vib} is the characteristic vibrational energy. The $\alpha_{sp}(\omega)$ term gives the absorption coefficient per unit small-polaron *density*. The spectrum is quite characteristic, exhibiting a broad asymmetric resonance which peaks at an excitation energy $\hbar\omega = 2E_b$ for a small polaron and $4E_b - U$ for an intrasite small bipolaron, where U is the on-site Coulomb repulsion energy [24,32]. For an intersite small bipolaron, i.e., a weakly-coupled two small polarons at adjacent sites, the absorption peaks at approximately $4E_b$ because U becomes negligible. An intersite scenario is applicable for the small bipolarons observed in this study as discussed later. Accordingly, to fit the absorption

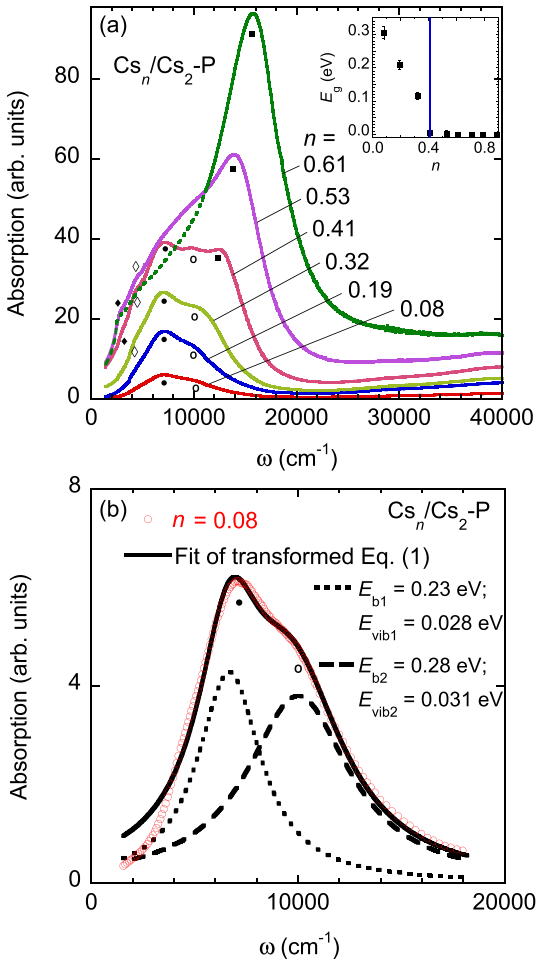

FIG. 2. The room-temperature optical properties of Cs_n/Cs_2-P. (a) The absorption spectra of $0.08 \leqslant n \leqslant 0.61$. The open and solid diamonds, solid and open circles, and solid squares mark the MIR1, MIR2, 6600, 10 500 cm^{-1}, and HF bands, respectively. The broken curve in $n = 0.61$ below 11 000 cm^{-1} indicate the spectral region where a reflectance is observed. The inset shows the n dependence of E_g. The vertical solid line in the inset indicates closing of E_g at $n = 0.41$. (b) The best fit of the small bipolaron absorption spectrum [transformed Eq. (1)] for $n = 0.08$ with two components.

bands at approximately 6600 and 10 500 cm^{-1}, we transform Eq. (1) to the small bipolaron spectrum by the substitution $2E_b \rightarrow 4E_b$ [24,32]. The fitting of $n = 0.08$ using two components ($E_{b1} = 0.23$ and $E_{b2} = 0.28$ eV) is shown in Fig. 2(b). Similar fits were obtained for $n \leqslant 0.41$ (samples for which the small bipolaron absorption bands are clearly discernible), and the fitting parameters are summarized in Table I. The fitting yields an n-independent E_b of $0.22 \sim 0.28$ eV. The two components E_{b1} and E_{b2} are, perhaps, due to the presence of two distinct excited states as argued later. This behavior is in contrast to the K and Rb counterparts [8,23], where a single absorption band is observed at comparable values of n.

At $n = 0.32$, a new band appears in the MIR region at approximately 3300 cm^{-1} (MIR1) and is marked by the open diamond in Fig. 2(a). At $n = 0.41$, additional bands appear at approximately 2600 (MIR2) and 12 500 cm^{-1} (HF), and are marked by the solid diamond and square, respectively.

TABLE I. The parameters used to fit the small bipolaron absorption spectrum given by transformed Eq. (1) to optical absorption bands at approximately 6600 and 10 500 cm^{-1} of $n = 0.08$, 0.19, 0.32, and 0.41.

n	E_{b1} (eV)	E_{vib1} (eV)	E_{b2} (eV)	E_{vib2} (eV)
0.08	0.23 ± 0.02	0.028 ± 0.004	0.28 ± 0.02	0.031 ± 0.003
0.19	0.22 ± 0.02	0.030 ± 0.002	0.27 ± 0.04	0.029 ± 0.005
0.32	0.23 ± 0.01	0.031 ± 0.003	0.26 ± 0.03	0.033 ± 0.002
0.41	0.23 ± 0.03	0.032 ± 0.003	0.28 ± 0.03	0.030 ± 0.004

These coexist with the MIR1 and small bipolaron bands (6600 and 10 500 cm^{-1}). With a further increase in n (= 0.53), the bands at approximately 6600 and 10 500 cm^{-1} assigned to small bipolaron absorptions become less discernible. In contrast, the MIR2 band becomes clearer and the HF band increases in intensity with a blueshift. At $n = 0.61$, the small bipolaron bands disappear, and a decrease in the absorption is observed in the spectral region approximately below 11 000 cm^{-1} as denoted by the broken curve in Fig. 2(a). A normal reflectance is applicable in this spectral region [30] of $n = 0.61$. Similar behavior is observed for $n = 0.71$, 0.79, and 0.87 [not shown in Fig. 2(a)]. The samples with $n = 0.08$ and 0.19 are insulating as confirmed by the exponentially decreasing absorption tails. The insulating gap E_g is estimated for $n \leqslant 0.53$ using the intercept of the straight line in the low-energy rise of $h\nu$ vs $[(k/s)h\nu]^2$ plots [33], where $h\nu$ is the photon energy. The n dependence of E_g is shown in the inset of Fig. 2(a). E_g decreases continuously and closes (within the error) at $n = 0.41$. For $n \geqslant 0.61$, as discussed below, a Drude component is observed, which is interpreted as a transition to a polaronic metal following the closing of E_g. Therefore, at $n \geqslant 0.61$, a closed E_g is indicated in the inset of Fig. 2(a) without resorting to any fitting procedure.

At $n = 0.61$, a normal reflectance is observed below 11 000 cm^{-1} and the absorptions at approximately 6600 and 10 500 cm^{-1} disappear [see Fig. 2(a)], transferring spectral weight to a Drude component. This behavior has been elusive at comparatively stronger coupling in this model system [8,23]. The reflectance spectra of $n \geqslant 0.61$ are shown in Fig. 3 for the spectral region below 11 000 cm^{-1}. The Drude component is superimposed on a MIR sideband [refer to the Drude-Lorentz (DL) analysis below]. This feature is denoted by the arrow in Fig. 3. The broken lines above 11 000 cm^{-1} denote that an absorption is applicable in the high frequency region. The inset of Fig. 3 shows the n dependence of reflectance at 2500 cm^{-1}.

The DL analysis was performed on $n \geqslant 0.61$ using the complex dielectric function

$$\varepsilon(\omega) = \varepsilon_\infty - \frac{\omega_p^2}{\omega^2 + i\omega/\tau} + \sum_j \frac{S_j^2}{\omega_j^2 - \omega^2 - i\omega\gamma_j}, \qquad (2)$$

where ε_∞ is the high-frequency dielectric constant, ω_p is the Drude plasma frequency, τ is the free-carrier relaxation time, and S_j and γ_j are the strength and spectral width of the Lorentz oscillators that peak at finite frequencies ω_j. The DL fits for the reflectance curves of $n = 0.61$, 0.71, 0.79, and 0.87 are shown in Figs. 4(a)–4(d). These give a Drude contribution plus two Lorentz oscillators in all four

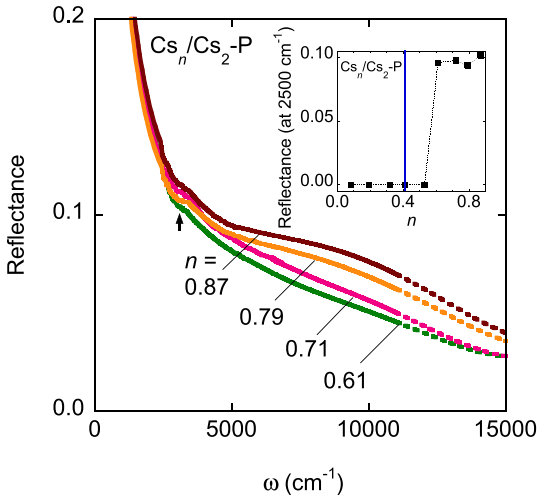

FIG. 3. The reflectance spectra of $n \geqslant 0.61$. The broken curves indicate that an absorption is applicable in the high-frequency region ($> 11\,000\,\mathrm{cm}^{-1}$). The arrow features the MIR sideband. The inset shows the n dependence of the reflectance at $2500\,\mathrm{cm}^{-1}$ for $n \leqslant 0.87$. The vertical solid line in the inset marks the closing of E_g at $n = 0.41$.

samples. For instance, the DL fit of $n = 0.61$ gives a Drude component (characterized by $\omega_p = 4330\,\mathrm{cm}^{-1}$ and a scattering rate $\Gamma = 9650\,\mathrm{cm}^{-1}$) and two Lorentzian oscillators, one in the MIR region at approximately 1200 (ω_1) and the other in the high-frequency region at approximately $16\,300\,\mathrm{cm}^{-1}$ (ω_2). The fitting parameters for $n \geqslant 0.61$ are summarized in Table II. In all four samples the Drude component is superimposed on the oscillator in the MIR region, suggesting that a simple

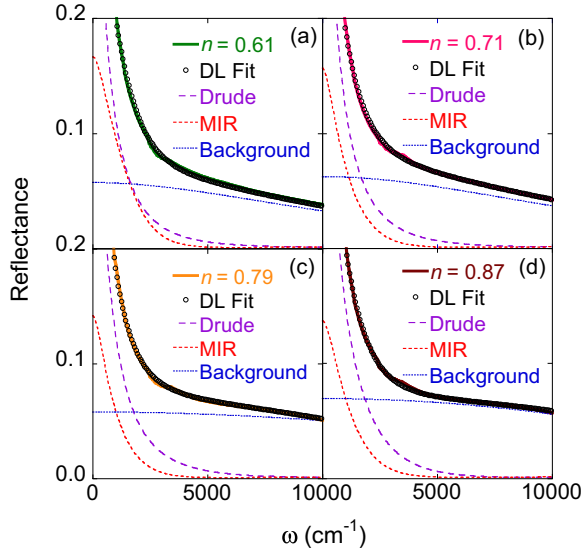

FIG. 4. The Drude-Lorentz fits [Eq. (2)] of reflectance spectra pertaining to n = (a) 0.61, (b) 0.71, (c) 0.79, and (d) 0.87. The experimental curves are represented by the solid lines. The fits of Eq. (2) are represented by the open circles. The individual fitting components describing the Drude term, MIR band, and high-frequency background are represented by the long dash, short dash, and dotted curves, respectively.

TABLE II. The Drude-Lorentz fitting parameters used to fit the optical reflectance spectra of $n \geqslant 0.61$ shown in Figs. 4(a)–4(d). The m^*/m values give the estimated electronic mass-enhancement (see the text for details).

n	ω_p (cm^{-1})	Γ (cm^{-1})	ω_1 (cm^{-1})	ω_2 (cm^{-1})	m^*/m
0.61	4330	9650	1205	16 341	1.83 ± 0.21
0.71	4630	10265	1204	16 021	1.78 ± 0.29
0.79	4635	10098	1175	15 995	1.72 ± 0.22
0.87	4013	6599	1300	15 988	1.79 ± 0.16

Drude term (a conventional metallic phase) does not explain the charge dynamics in the conducting phase observed at $n \geqslant 0.61$ [25,26]. The appearance of a polaronic metal characterized by a Fröhlich polaron [25,28] is discussed later. The second oscillator centered at approximately $16\,300\,\mathrm{cm}^{-1}$ at $n = 0.61$ reproduces the high-frequency background observed in these samples. The origin of this background is unclear.

The Curie-Weiss analysis of the temperature dependence of the magnetic susceptibility of Cs$_n$/Cs$_2$-P (not shown here), similar to Na, K, and Rb counterparts [8,23], gives a small Curie constant C (highest being 0.51×10^{-4} K emu/cm^3 at $n = 0.87$). At 100% occupancy of a localized spin $S = \frac{1}{2}$ in each GIS cage, C is 2.44×10^{-3} K emu/cm^3. This suggests that in all samples the majority of guest electrons (>98%) are in a paired state. A minority of unpaired states carry a magnetic moment $S = \frac{1}{2}$, highlighting the presence of a weak disorder even at high electron densities.

IV. DISCUSSION

In a periodic ionic lattice, an electron with finite transfer energy is itinerant, according to the tight-binding model. However, Frank-Condon displacements in the lattice due to short-range electron-lattice coupling result in self-trapped carriers [7,34] and large fluctuations in the electronic potential opening a mobility gap. Insulating ($E_g \approx 0.3$ eV at $n = 0.08$) and nonmagnetic (low C) phase at $n < 0.41$ with characteristic absorption bands [24] at approximately 6600 and 10 500 cm^{-1} is attributed to the formation of isolated small bipolarons due to Frank-Condon displacements. The splitting of the small bipolaron absorption band is perhaps due to two distinct optically excited states as explained below. The excitation of a self-trapped electron out of the deformation potential results in a temporary unbound state with wavelength comparable to the lattice constant(s) [24]. In zeolite P, $a = 14.2386(5)$ and $b = 9.9836(3)$ Å (see Fig. 1) [22]. Unbound electrons with wavelengths of 14 Å ($\approx a$) and 10 Å ($\approx b$) have kinetic energies of 0.8 eV ($\approx 6500\,\mathrm{cm}^{-1}$) and 1.4 eV ($\approx 11\,000\,\mathrm{cm}^{-1}$), respectively, with remarkable agreement with the observed bands. Therefore, the two components at approximately 6600 and 10 500 cm^{-1} of the small bipolaron band is assigned to two distinct excited states along the a and b axes, respectively.

The peak positions of the small bipolaron bands remain constant and discernible to $n = 0.41$ indicating an increase in the number density of small bipolarons. Near $n = 0.41$, drastic changes are observed in the optical properties. The

MIR1, MIR2, and HF bands appear and E_g closes. To explain these changes, we resort to percolation of small bipolarons. As illustrated in Fig. 1, cage voids form a diamond lattice. The site-percolation threshold proposed for paired constituents in the diamond lattice is 0.35 [35]. For intersite small bipolarons, percolation occurs around this threshold (corresponding $n \approx 0.35$) leading to weak localization effects due to the relaxation of lattice deformations induced by isolated small bipolarons [23]. This closes E_g and sets in many-electron(polaron) effect, likely in a polaron Wigner-lattice [27,36]. The HF band, in a weakly localized scenario, is ascribed to surface plasmon excitations along the c axis. The electron density n_e at $n = 0.5$ is $\approx 0.4 \times 10^{22}$ cm^{-3} (considering the volume ratio of cavities [22]). At $n = 0.5$, the surface plasmon energy estimated using an analogy with bulk Cs metal is 1.8 eV ($\approx 14\,500$ cm^{-1}), and is in close agreement with the HF band observed at approximately 14 000 cm^{-1} at $n = 0.53$. The HF band continues to grow with a blueshift to $n = 0.87$ (evolution of the HF band is shown only up to $n = 0.61$ in Fig. 2(a) to maintain visibility of other bands). The oscillator strength and the energy of the surface plasmon increase with n_e (or n), consistent with the evolution of the HF band with increasing n.

The MIR1 band appears at $n = 0.32$ near the percolation threshold [35]. Similar behavior was observed in the Rb system [23]. Electron-lattice coupling gives rise to "incoherent" contributions, resulting in absorptions in the MIR region as observed in other polaron materials [26,37,38]. In this scenario, the MIR1 band is ascribed to photo-induced hopping of small bipolarons between adjacent self-trapped states [23,24,38]. At $n = 0.41$, the MIR2 band appears coinciding with the closing of E_g. This behavior in the optical properties of Cs_n/Cs_2-P at $n = 0.41$ is consistent with the behavior observed at the transition to extended states in the Rb system, although, at a much higher value of n (= 0.89) [23]. Hence, the MIR2 band is imputed to incoherent transport of extended states [23,24,26,37]. The onset of the weak-limit of W due to percolation and consequent relaxations in the deformed lattice closes the mobility gap introducing extended states at the Fermi energy [16].

We observe a "melting phase" of small bipolarons above the mobility edge ($0.41 \leqslant n < 0.61$). Competing bands pertaining to small bipolarons (self-trapped) and extended states (MIR2) coexist at $n = 0.41$. However, with a further increase in n (= 0.53), features of the small bipolaron band become less discernible, while the MIR2 band becomes clearer [see Fig. 2(a)]. A two-fluid (mixed phase) model [23,39] is applicable in explaining the transport in this region ($0.41 \leqslant n < 0.61$), which must reflect a nontrivial interplay of dynamical lattice deformations, relaxations, and W [16,40].

At $n = 0.61$, the small bipolarons dissociate due to increasing density in a polaron Wigner-lattice [27,41] (evident by the disappearance of bands at 6600 and 10 500 cm^{-1}), resulting in the appearance of a Drude component superimposed on a MIR sideband. The spectral weight distribution between coherent (Drude) and incoherent (MIR) contributions indicates the polaronic nature of charge carriers in this itinerant phase ($n \geqslant 0.61$). The MIR and Drude intensities at room temperature can be used to estimate the polaronic mass m^* [25,26,37]. The mass-renormalization factor of the charge carriers is defined by $m^*/m = (SW_{MIR} + SW_{Drude})/SW_{Drude}$, where SW_{MIR} and SW_{Drude} are the electronic spectral weights

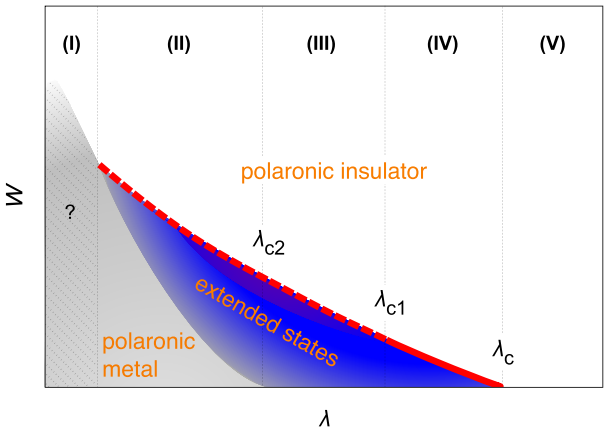

FIG. 5. Phase diagram for the metal-insulator transition in a deformable lattice in the face of electron-lattice coupling and a random electronic potential. Above λ_c [16], a mobility gap is open even at weak W. λ_{c1} ($< \lambda_c$) is the coupling strength above which the transition to extended states is discontinuous. λ_{c2} is the coupling strength above which the transition to extended states is continuous, and below which a further transition from extended states to a polaronic metal manifests as $W \rightarrow 0$. The red broken and solid lines denote a continuous and discontinuous transition, respectively.

(calculated by integrating the real part of the optical conductivity obtained from DL-fitting parameters) of the MIR and Drude components, respectively. A n-independent mass enhancement of roughly twofold is observed. The m^*/m values are summarized in Table II. To estimate the coupling constant α in this phase, we resort to the Feynman's relation $m^*(\alpha)$ deduced within a variational approximation [28]. Application of the experimental m^* values to $m^*(\alpha)$ valid in the range $0 < \alpha < 12$ yields an n-independent value $3 < \alpha < 4$ ($\alpha \approx 3.3$) in close agreement with $\alpha = 3.6$ for a Fröhlich polaron in a polar medium [25]. With increasing small bipolaron density, we observe a transition to a polaronic metal characterized by a Fröhlich polaron [42] at $n \geqslant 0.61$ (an unbound state, but with long-range electron-lattice coupling [24]). This has been elusive at stronger λ in this model system [8,23].

In Fig. 5 we illustrate the phase diagram established experimentally for the metal-insulator transition in a deformable lattice in the face of electron-lattice coupling and a random electronic potential. In partial agreement with a recent theory [16], Cs_n/Cs_2-P shows a continuous transition to a polaronic metal (in contrast to the suggested conventional metal). This transition falls within region II of Fig. 5. At comparatively stronger λ, a continuous conducting transition from insulating to extended states was proposed [16]. We observed this continuous transition above a critical coupling strength λ_{c2} for the Rb system [23], which falls within region III. Interestingly, we also observed a discontinuous transition above a coupling strength λ_{c1} (region IV) for the K system [8], suggesting the presence of a region of λ for which the transition is discontinuous in agreement with Cohen *et al.* [13,19]. Region V is a stubborn polaronic insulator, where a mobility gap is open irrespective of the magnitude of W due to strong λ as observed for the Na system [23]. Several key issues remain unresolved. Other driving parameters, their interactions, and detailed energy scales (λ_c, λ_{c1}, and λ_{c2}) are yet to be established. The transition

to a conventional metal and possibly superconductivity due to dissociation in a polaron Wigner lattice [27] remains elusive, and we represent this in the hypothetical region I. High pressure studies and (or) weaker λ are of interest in this regard.

In summary, a continuous (polaronic) metal-insulator transition is observed in this model system revealing an important part of the complex phase diagram. The insulating and nonmagnetic phase together with the characteristic optical response indicate the formation of small bipolarons. The percolation of small bipolarons and consequent weak limit of disorder in the electronic potential result in a melting phase of small bipolarons. Subsequent disappearance of small bipolarons gives way to a polaronic metal evidenced by a Drude component superimposed on a MIR sideband. Approximately a twofold mass enhancement yields a coupling constant that suggests a Fröhlich polaron in this itinerant phase. Further investigations in this direction have the potential to explain many puzzling properties of disordered metals.

ACKNOWLEDGMENTS

We thank Y. Nozue, T. Nakano, and S. Tamiya for providing experimental facilities and assistance. G.P.H. thanks M. S. Osofsky for stimulating discussions. G.P.H. acknowledges financial support from the Research Promotion Division of Osaka University and the Ministry of Education, Culture, Sports, Science and Technology of Japan under the program for promoting research activities and enhancement of research universities.

[1] L. D. Landau, Phys. Z. Sowjet. **3**, 664 (1933).
[2] N. F. Mott, Adv. Phys. **39**, 55 (1990).
[3] A. Bussmann-Holder and H. Keller, J. Supercond. Nov. Magn. **22**, 123 (2009).
[4] H. M. Rønnow, C. Renner, G. Aeppli, T. Kimura, and Y. Tokura, Nature **440**, 1025 (2006).
[5] J. T. Devreese and S. A. Alexandre, Rep. Prog. Phys. **72**, 066501 (2009).
[6] J. J. Lee, F. T. Schmitt, R. G. Moore, S. Johnston, Y. Y. Cui, W. Li, M. Yi, Z. K. Liu, M. Hashimoto, Y. Zhang, D. H. Lu, T. P. Devereaus, D. H. Lee, and Z. X. Shen, Nature **515**, 245 (2014).
[7] C. Jooss, L. Wu, T. Beetz, R. F. Klie, M. Beleggia, M. A. Schofield, S. Schramm, J. Hoffmann, and Y. Zhu, Proc. Natl Acad. Sci. USA **104**, 13597 (2007).
[8] G. P. Hettiarachchi, T. Nakano, Y. Masaki, M. N. M. Muhid, H. Hamdan, and Y. Nozue, J. Phys. Soc. Jpn. **84**, 014702 (2015).
[9] T. Nakano and Y. Nozue, Adv. Phys. X **2**, 254 (2017).
[10] D. Emin, Comments Solid State Phys. **11**, 35 (1983).
[11] K. P. McKenna, M. J. Wolf, A. L. Shluger, S. Lany, and A. Zunger, Phys. Rev. Lett. **108**, 116403 (2012).
[12] H. Shore, L. Sander, and L. Kleinman, Nature (London), Phys. Sci. **245**, 44 (1973).
[13] M. H. Cohen, E. N. Economou, and C. M. Soukoulis, Phys. Rev. Lett. **51**, 1202 (1983).
[14] Y. Shinozuka, J. Non-Cryst. Solids **77-78**, 21 (1985).
[15] P. W. Anderson, Nat. Phys. Sci. (London) **235**, 163 (1972).
[16] D. Di Sante, S. Fratini, V. Dobrosavljević, and S. Ciuchi, Phys. Rev. Lett. **118**, 036602 (2017).
[17] P. A. Lee and T. V. Ramakrishnan, Rev. Mod. Phys. **57**, 287 (1985).
[18] F. Evers and A. D. Mirlin, Rev. Mod. Phys. **80**, 1355 (2008).
[19] M. H. Cohen, E. N. Economou, and C. M. Soukoulis, Phys. Rev. B **29**, 4496 (1984).
[20] D. Emin and T. Holstein, Phys. Rev. Lett. **36**, 323 (1976).
[21] E. Abrahams, P. W. Anderson, D. C. Licciardello, and T. V. Ramakrishnan, Phys. Rev. Lett. **42**, 673 (1979).
[22] B. R. Albert, A. K. Cheetham, J. A. Stuart, and C. J. Adams., Microporous Mesoporous Mater. **31**, 253 (1999).
[23] G. P. Hettiarachchi, F. Moriasa, Y. Nishida, T. Nakano, Mohd Nazlan Mohd Muhid, and H. Hamdan, Phys. Rev. B **96**, 155115 (2017).
[24] D. Emin, Phys. Rev. B **48**, 13691 (1993).
[25] J. L. M. van Mechelen, D. van der Marel, C. Grimaldi, A. B. Kuzmenko, N. P. Armitage, N. Reyren, H. Hagemann, and I. I. Mazin, Phys. Rev. Lett. **100**, 226403 (2008).
[26] L. Baldassarre, A. Perucchi, E. Arcangeletti, D. Nicoletti, D. Di Castro, P. Postorino, V. A. Sidorov, and S. Lupi, Phys. Rev. B **75**, 245108 (2007).
[27] S. Fratini and P. Quémerais, Eur. Phys. J. B **14**, 99 (2000).
[28] R. P. Feynman, Phys. Rev. **97**, 660 (1955).
[29] P. Kubelka and F. Munk, Z. Tech. Phys. **12**, 593 (1931).
[30] T. Kodaira, Y. Nozue, S. Ohwashi, T. Goto, and O. Terasaki, Phys. Rev. B **48**, 12245 (1993).
[31] H. G. Reik and D. Heese, J. Phys. Chem. Solids **28**, 581 (1967).
[32] A. V. Puchkov, T. Timusk, M. A. Karlow, S. L. Cooper, P. D. Han, and D. A. Payne, Phys. Rev. B **52**, R9855 (1995).
[33] E. A. Davis and N. F. Mott, Philos. Mag. **22**, 903 (1970).
[34] Y. Toyozawa, Prog. Theor. Phys. **26**, 29 (1961).
[35] H. Holloway, Phys. Rev. B **37**, 874 (1988).
[36] K. Arya, Z. B. Su, and J. L. Birman, Phys. Rev. Lett. **54**, 1559 (1985).
[37] L. V. Gasparov, D. B. Tanner, D. B. Romero, H. Berger, G. Margaritondo, and L. Forro, Phys. Rev. B **62**, 7939 (2000).
[38] A. Perucchi, L. Baldassarre, A. Nucara, P. Calvani, C. Adamo, D. G. Schlom, P. Orgiani, L. Maritato, and S. Lupi, Nano Lett. **10**, 4819 (2010).
[39] V. V. Kabanov and D. K. Ray, Phys. Rev. B **52**, 13021 (1995).
[40] M. S. Osofsky, C. M. Krowne, K. M. Charipar, K. Bussmann, C. N. Chervin, I. R. Pala, and D. R. Rolison, Sci. Rep. **6**, 21836 (2016).
[41] G. Iadonisi, V. Mukhomorov, G. Cantele, and D. Ninno, Phys. Rev. B **76**, 144303 (2007).
[42] G. Rastelli and S. Ciuchi, Phys. Rev. B **71**, 184303 (2005).